

Three Dimensional Cone-beam Reconstruction of Micro Computed Tomography in the Breast Specimen

Ho-Shiang Chueh Jyh-Cheng Chen* Ing-Tsung Hsiao¹ Yuh-Ren Shieh²

Institute of Radiological Sciences, National Yang-Ming University, Taipei, 112, Taiwan R.O.C.

¹*School of Medical Technology, Chang Gung University, Tao-Yuan, 330, Taiwan R.O.C.*

²*Biomedical Eng. Center, Industrial Technology Research Inst., Hsinchu, 300, Taiwan R.O.C.*

Received 12 May 2004; Accepted 3 June 2004

Abstract

Traditionally, the specimen obtained from a breast biopsy can only be examined by a microscope. Although the resolution of microscope is high, it can only examine one thin section at a time. Hence, the microcalcifications next to the observed section may be missed. To solve for this problem, we acquire the specimen by a 3D micro computed tomography (microCT) with electron bombarded charged coupled device (EBCCD). The objective of this study was to implement and evaluate the 3D cone-beam reconstruction algorithms for the breast specimen using microCT. We have reconstructed the projections of specimen by parallel-beam, fan-beam, and cone-beam algorithms. For the cone-beam algorithm, we used the tent Feldkamp-Davis-Kress method (T-FDK) in this research. To evaluate the performance, we computed the coefficient of variation (CV) and contrast in the reconstructed images obtained from a cubic phantom, and analyzed the result by a t-test. From the results, we found that significant advantage of T-FDK over others. For the breast specimen, the microcalcifications can be easily identified in the images reconstructed using the T-FDK algorithm, but not in those reconstructed from the filtered backprojection (FBP). We then displayed these reconstructed images in 3D, and applied a 3D computer-aided diagnosis tool for classifying breast cancer. However, there are still some artifacts caused by these analytical reconstruction methods. For the future work, we plan to apply statistical iterative reconstruction methods in the microCT reconstruction, and expect the statistical reconstruction methods can reduce these artifacts.

Keywords: Cone-beam, Breast cancer, T-FDK algorithm, MicroCT, 3D reconstruction

Introduction

In present research, single photon emission computed tomography (SPECT) with a cone-beam collimator has been under investigation for several years [1, 2]. The main advantages of using a cone-beam collimator are the gain in sensitivity and resolution over images formed using standard parallel-hole or fan-beam collimators [3, 4]. In cone-beam X-ray medical imaging and non-destructive testing, a two-dimensional detector is used to speed up the data acquisition and improve the sensitivity. The X-ray source defines the cone-beam focal point, and an image intensifier can be used as a two-dimensional defector [5]. The FDK algorithm, a filtered backprojection (FBP) based reconstruction method, was derived to reconstruct the cone-beam projections from mathematical and physical phantoms [6]. It is considered a suitable cone-beam reconstruction algorithm for the microCT. However, it has

rarely been applied to real objects. In this study, we implemented a modified FDK algorithm [7], called T-FDK algorithm, and used it to reconstruct the cone-beam projection data acquired from the microCT. This microCT scanner was assembled by the Industrial Technology Research Institute (ITRI), and it used a high-resolution EBCCD detector with an X-ray generator. We acquired a specimen data from a breast biopsy, and then applied the T-FDK algorithm. The reconstruction from the T-FDK method was compared to that using a parallel-beam filtered backprojection reconstruction algorithm.

Materials and Methods

MicroCT

The microCT made by the ITRI contains a high-frequency X-ray generator with a mini focus X-ray tube and the EBCCD detector. The focal spot of the X-ray tube is 1 mm². The EBCCD detector has a square field of view (FOV) of 55.5*55.5 mm² and is able to acquire projections for a matrix of 1040*1040. An object was placed on a rotating stage

*Corresponding author: Jyh-Cheng Chen
Tel: +886-2-28267282; Fax: +886-2-28201095
E-mail: jcchen@ym.edu.tw

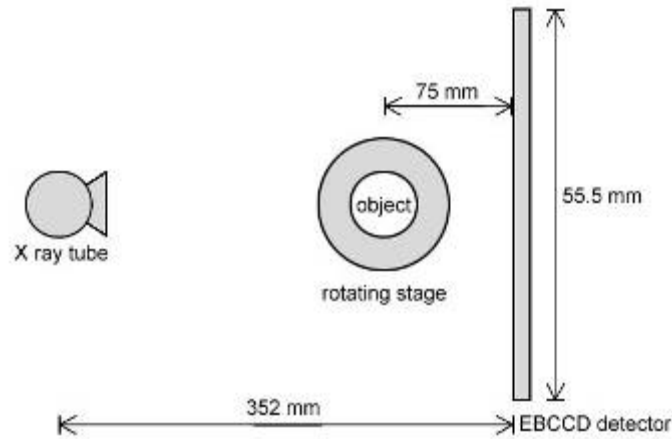


Figure 1: The illustration of devices in the micro CT system. The specimen was put on the rotating stage and was exposed 400 exposures over 360 degree to acquire projections. The EBCCD has a square FOV of 55.5*55.5 mm². The distance from focus spot to detector is 352 mm. The distance from center of rotating stage to detector is 75 mm.

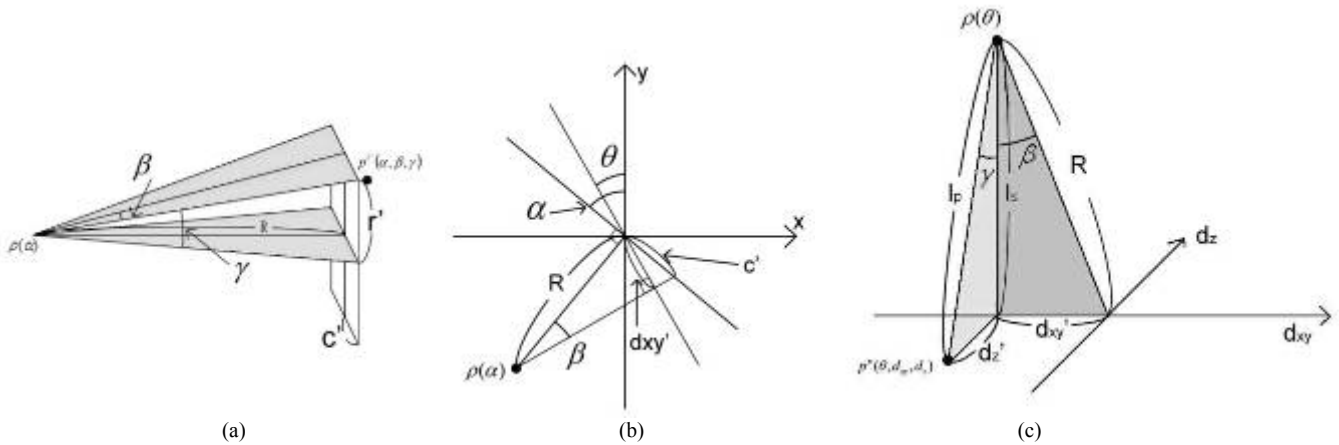


Figure 2: The diagram shows the geometry relationship of the parameters. (a) and (b) are the diagrams to show the coordinates for real cone-beam projection data. θ is an angle of the the virtual parallel-beam projection. c, r are column and row coordinates of detector, respectively. c', r' are specific c, r , respectively. α is an angle between normal of source and detector system. β and γ are fan and cone angles, respectively. R is the distance of source to the detector. $\rho(\alpha)$ is a source position. (c) is the diagram to show the coordinates for virtual parallel-beam projection data. d_{xy} and d_z are column and row coordinates of the virtual parallel-beam detector, respectively. d_{xy}' and d_z' are specific d_{xy} and d_z , respectively. $\rho(\theta)$ is an extended source position.

and was exposed 400 exposures over 360 degrees to acquire projections in one scan. The distance from focal spot to detector was 352 mm (see Figure 1), which was measured by investigating the projection data. Before obtaining projections, a blank scan was acquired for the compensation of non-uniform effect from the detector.

T-FDK

In the T-FDK algorithm, the cone-beam projection data ($p^C(\alpha, \beta, \gamma)$) was transformed to virtual parallel-beam projection data ($p^P(\theta, d_{xy}, d_z)$) by parallel rebinning step [7]. The geometry of these parameters is shown in Figure 2. In the horizontal plane, the real cone beam projection coordinates (α and β) can be exactly transferred to the virtual parallel coordinates. It can be expressed here as

$$\theta = \alpha - \beta, \quad d_{xy}' = R \sin \beta \tag{1}$$

, or equivalently

$$\alpha = \theta + \beta, \quad \beta = \arcsin \frac{d_{xy}'}{R} \tag{2}$$

For a flat panel detector like EBCCD, the β above should be replaced by

$$\beta = \arctan \frac{c'}{R} \tag{3}$$

In vertical plane, the virtual coordinate can be expressed by

$$d_z' = R \tan(\gamma) \cos(\beta) \tag{4}$$

For compensating the different ray length through the volume, a two-dimensional cosine type weighting function was

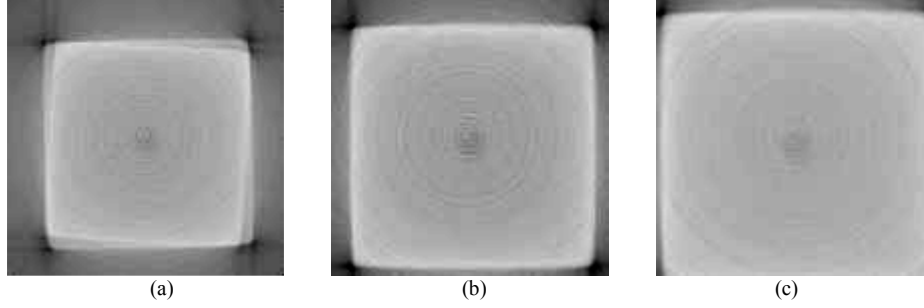


Figure 3: (a), (b) and (c) are the images reconstructed by parallel-beam, fan-beam and cone-beam reconstruction, respectively. The image reconstructed by parallel-beam shows an obvious blur due to an error of fan-angle.

used:

$$w(d_{xy}, d_z) = \cos(\gamma(d_{xy}, d_z)) = \frac{l_s}{l_p} \quad (5)$$

, where the l_s is the height of the extended source position ($\rho(\theta)$) over the central line of the virtual detector. It is described by $l_s = \sqrt{R^2 - d_{xy}^2}$. The l_p is the length of the ray from the extended source position to the pixel under consideration. It is described by $l_p = \sqrt{l_s^2 + d_z^2}$. Finally, the p^p can be rapidly reconstructed by parallel-beam convolution backprojection (CBP) as

$$f(x, y, z) = \frac{1}{2\pi} \int_0^{2\pi} \left[p^p(\theta, d_{xy}, d_z) \cdot w(d_{xy}, d_z) \right] * h(d_{xy}) d\theta \quad (6)$$

, where the $h(d_{xy})$ is an one dimensional band limited ramp filter.

Phantom study

A cubic phantom was used to evaluate difference among parallel-beam, fan-beam and cone-beam reconstructions. Tomographic images were reconstructed by the three reconstruction methods from the same set of projections. After the reconstruction, we then displayed the reconstructed images in 3D view using a surface rendering method. To compare the above three reconstructions, we computed the coefficient of variation (CV), and contrast was measured in regions of interest (ROIs) in the same horizontal position. CV is defined by a ratio of standard deviation (SD) of grey level of points in a ROI to a mean of grey level of points in a ROI. Contrast is defined by a ratio of absolute value of a difference that is between mean gray level of object in the ROI and mean gray level of background in the ROI to an absolute value of mean gray level of background. These values were analyzed and compared to each other by the Student's t-test.

Specimen study

A specimen obtained in mastectomy was put in a plastic bottle filled with formalin. The bottle was then put on the rotating stage to acquire planar projections of the specimen. These projection data were reconstructed by both parallel and cone-beam reconstructions. The reconstructed images can be displayed on any section and any surface by surface rendering. We applied a computer-aided detection (CAD) program on the

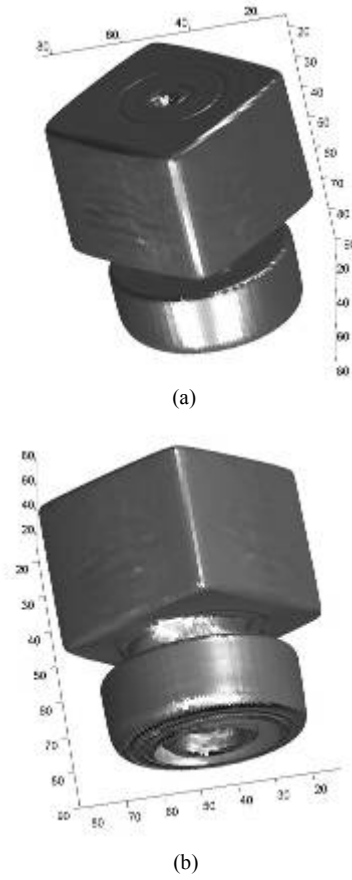


Figure 4: 3D display of the cubic phantom. The volume data is displayed by surface rendering. We can observe the global object to view the specific surface of interest.

reconstructed images. The CAD program was used to assist in detecting possible regions of the microcalcifications. We utilized a graphic user interface (GUI) to show the 3D image and the 3D possible regions of the microcalcifications.

Results and Discussion

The reconstructed images of the cubic phantom from the three reconstruction methods are shown in Figure 3. These images were not in the middle section of the phantom, i.e., there is fan angle and small cone angle. The image reconstructed by parallel-beam FBP shows an obvious blur due to an error of fan angle. The images reconstructed by fan-beam

Table 1. This table shows the comparisons of CV and contrast that were measured in the same region among the images obtained by parallel, fan-beam and cone-beam reconstruction methods. The P value was the result of Student's t-test.

(a) Comparison between images obtained by parallel and fan-beam reconstructions.			
	Parallel-beam	Fan-beam	P value
CV	0.2015	0.1988	P = 0.1920
contrast	2.8902	2.8662	P = 0.2298

(b) Comparison between images obtained by parallel and cone-beam reconstruction.			
	Parallel-beam	Cone-beam	P value
CV	0.2015	0.1663	P = 0.0017
contrast	2.8902	2.9844	P < 0.0001

(c) Comparison between images obtained by fan and cone-beam reconstruction			
	Fan-beam	Cone-beam	P value
CV	0.1988	0.1663	P = 0.0058
Contrast	2.8662	2.9844	P < 0.0001

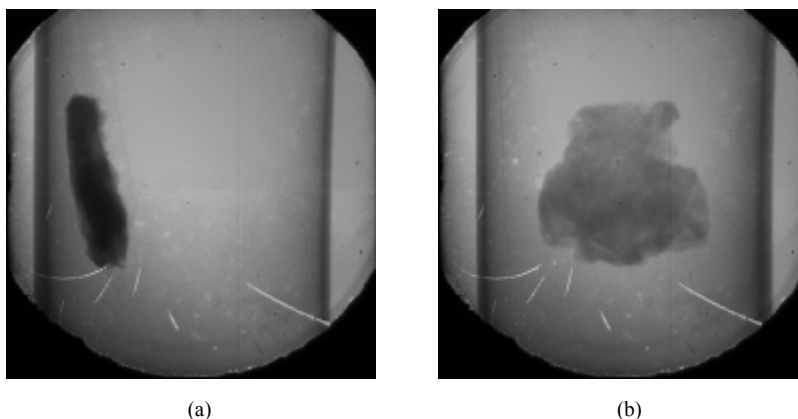


Figure 5: The planar projections acquired by the EBCCD, (a) is projection in 0° direction. (b) is projection in 90° direction. The specimen obtained from mastectomy was put in a plastic bottle filled with formalin.

and cone-beam show not much difference because the cone-angle is small in our configuration. The reconstructed result was a volume data. It not only can be displayed in sectional images, but also can be displayed in other methods, such as surface rendering, maximum intensity projection and volume rendering. Figure 4 shows a surface rendering of the phantom images. The CV and contrast in the ROIs among all reconstructed results were shown in Table 1. These results are compared by the Student's t test. From the preliminary results, one can see the effectiveness of the T-FDK reconstruction on the cone-beam projection data from the physical phantom. Also, the images reconstructed by cone-beam algorithm show a statistically significant improvement as compared to the parallel and fan-beam algorithms.

The projections of the specimen were acquired by the EBCCD (see Figure 5) and reconstructed by the parallel-beam and cone-beam reconstructions. Then, we reformatted the tomograms to observe the specimen in axial, coronal and sagittal view (see Figure 6). We can easily recognize the microcalcifications in the tomograms, which were reconstructed by the cone-beam reconstruction; in contrast, we cannot discriminate the microcalcifications in the tomograms reconstructed by the other method because of blurring. The volume data of specimen was displayed by surface rendering to show the 3D distribution of the microcalcifications (shown in Figure 7). The microcalcification locations were defined

from the CAD program. Therefore, from the CAD results, we can observe the relative position and configuration of the microcalcifications.

In this experiment, we can observe a significant improvement from the results of the cone-beam reconstruction algorithm in terms of noise reduction and contrast enhancement of the specimen images in the axial, coronal and sagittal view.

Conclusions

We have implemented the T-FDK cone-beam reconstruction algorithm, and applied it to a physical phantom data, and a specimen data acquired from the microCT. The images reconstructed from the parallel-beam reconstruction method are blurring. In the images reconstructed by the T-FDK algorithm, the CV is lower and the contrast is higher in the reconstructed images of the cubic phantom. Our results show that the T-FDK cone-beam reconstruction method generate better image quality in terms of uniformity, and lesion detection as compared to others. The microcalcifications in the specimen can be recognized and located by visual inspection and the CAD program. In this research, a feasibility of the T-FDK algorithm for a real object in the microCT imaging has been demonstrated. Finally, we hope that more applications of cone-beam microCT will be developed in the future.

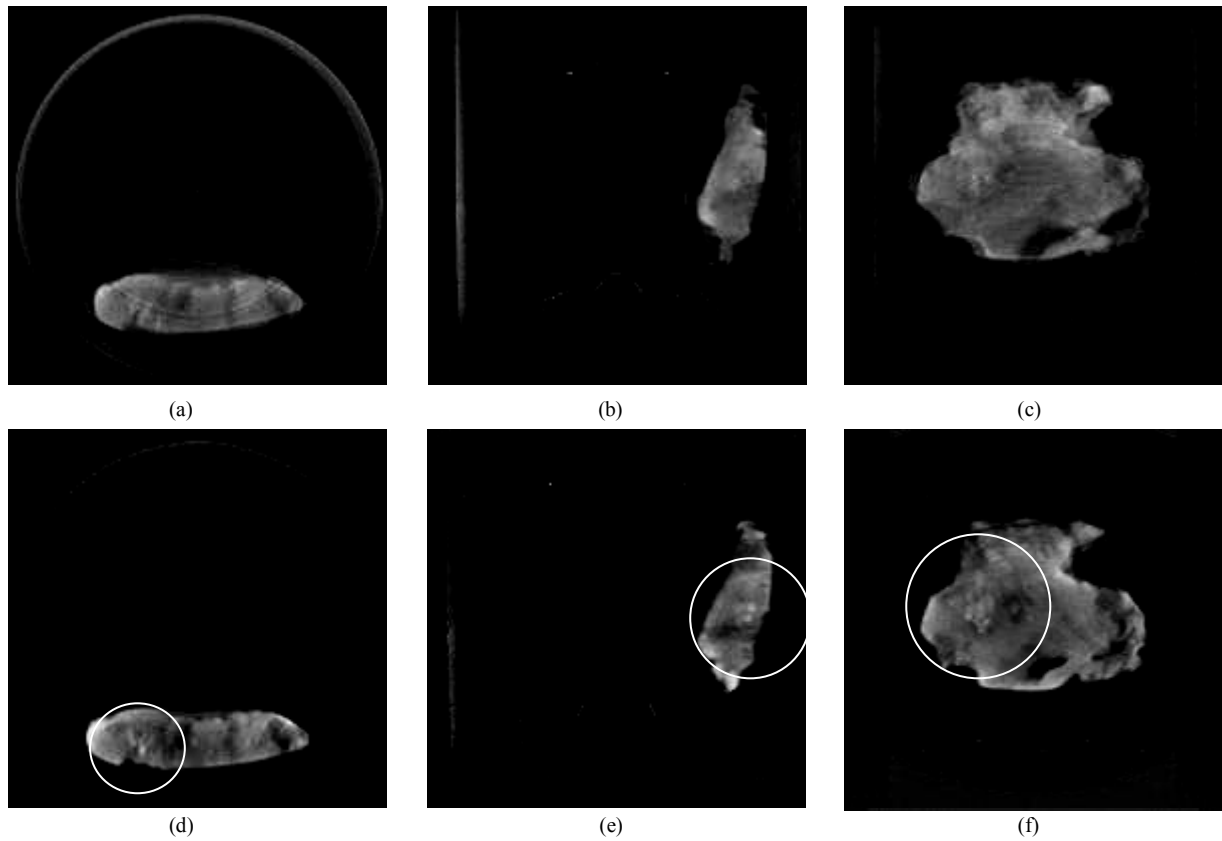
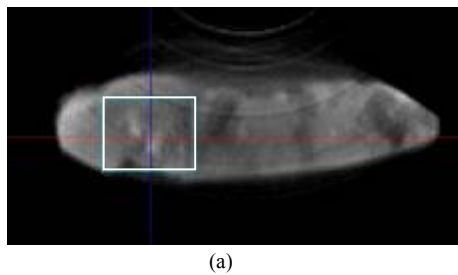
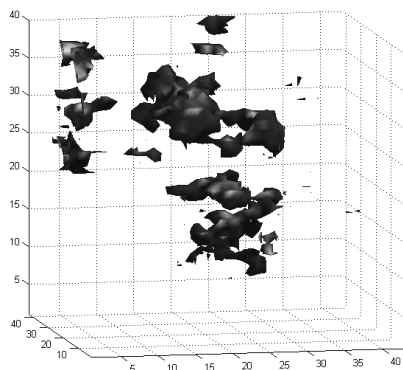


Figure 6: (a), (b) and (c) are the image reconstructed by parallel-beam FBP reconstruction in axial, sagittal and coronal view, respectively. (d), (e) and (f) are the image reconstructed by T-FDK algorithm in axial, sagittal and coronal view, respectively. The microcalcifications can be observed in the highlight region on images reconstructed by cone-beam reconstruction.



(a)



(b)

Figure 7: (a) is the region of interest. (b) microcalcifications in this region were displayed by surface rendering. The microcalcifications were defined by the CAD program. This result also shows that the specimen can be examined by various methods after reconstruction.

Acknowledgement

This study was supported by a grant (91GE03) from BMEC-ITRI.

References

- [1]. R. J. Jaszczak, C. E. Floyd, S. M. Manglos, K. L. Greer and R. E. Coleman, "Cone beam collimation for single photon emission computed tomography: analysis, simulation, and image reconstruction using filtered backprojection", *Med. Phys.*, 13: 484-9, 1986.
- [2]. R. J. Jaszczak, K. L. Greer and R. E. Coleman, "SPECT using a specially designed cone beam Collimator", *J. Nucl. Med.*, 29: 1398-1405, 1988.
- [3]. L. Z. Gengsheng and T. G. Grant, "A cone-beam tomography algorithm for orthogonal circle-and-line orbit", *Phys. Med. Biol.*, 37: 563-571, 1992.
- [4]. X. H. Yan and R. M. Leahy, "Cone beam tomography with circular, elliptical and spiral orbits", *Phys. Med. Biol.*, 37: 493-506, 1992.
- [5]. R. Ning, H. Hu and R. A. Kruger, "Image intensifier-based CT volume imager for angiography" SPIE Medical Imaging II Conf., Newport Beach, CA, SPIE 914: 282-90, 1988.
- [6]. L. A. Feldkamp, L. C. Davis and J. W. Kress, "Practical cone-beam algorithm", *J. Opr. Soc. Am. A* 1: 612-9, 1984.
- [7]. M. Grass, T. Köhler and R. Proksa, "3D cone-beam CT reconstruction for circular trajectories" *Phys. Med. Biol.*, 45: 329-347, 2000.

微型電腦斷層之三維錐狀射束影像重組在乳房檢體之應用

闕河翔 陳志成* 蕭穎聰¹ 謝育仁²

國立陽明大學放射醫學科學研究所

¹長庚大學醫事技術學系

²工業技術研究院生物醫學工程中心

收件日期 2004 年 5 月 12 日；接受日期 2004 年 6 月 3 日

摘 要

有關乳房組織切片檢體的檢查，在傳統上只能以顯微鏡的方式來檢查。雖然顯微鏡可以提供很好的空間解析度，但卻只能觀察到一個很薄的切面，因此，如果所欲觀察的微鈣化點不在這個切面的範圍之內，我們便無法觀察到它。為了解決這個問題，我們利用微型電腦斷層儀來對檢體取像，而這個微型電腦斷層儀是使用一個電子衝擊電荷耦合裝置來做為 X 光的偵檢器。這個研究的目的是在於研究三維錐狀射束微型電腦斷層造影術在乳房組織切片檢體的應用及評估。我們以平行射束、扇狀射束和錐狀射束三種不同的影像重組演算法來做檢體的影像重組，在這個實驗中，我們是以 tent Feldkamp-Davis-Kress method (T-FDK)來做為錐狀射束影像重組的演算法。我們從立方體假體的影像中以 t-test 分析影像的變異係數和對比度，發現以 T-FDK 演算法重組的影像有明顯的改進。在評估臨床的資料上，我們可以在使用 T-FDK 演算法的影像中很明顯的觀察到在檢體中的微鈣化點，而在使用一般濾波反投影法的影像中卻無法看到。而且我們可以將影像重構，以三維的方式來表現，並輔以三維的電腦輔助診斷，來幫助臨床上乳癌的診斷及分期。然而，還是有一些因為濾波反投影法造成的假影，我們希望將來可以利用統計式疊代重組法來減少相關的假影。

關鍵詞：錐狀射束、乳癌、T-FDK 演算法、微型電腦斷層儀、三維影像重組

* 通訊作者：陳志成
電話：+886-886-2-28267282； 傳真：+886-2-28201095
電子郵件信箱：jcchen@ym.edu.tw